# X-ray diffraction from CuPt-ordered III-V ternary semiconductor alloy films

J. H. Li,[1,2] J. Kulik,[2] V. Holý,[3] Z. Zhong,[1] S. C. Moss,[1] Y. Zhang,[4] S. P. Ahrenkiel,[4] A. Mascarenhas,[4] and Jianming Bai[5]
[1]*Physics Department, University of Houston, Houston, Texas 77204-5506*
[2]*Texas Center for Superconductivity, University of Houston, Houston, Texas 77204*
[3]*Department of Solid State Physics, Faculty of Science, Masaryk University, Kotlarska 2, 61137 Brno, Czech Republic*
[4]*National Renewable Energy Laboratory, Golden, Colorado 80401*
[5]*Oak Ridge National Laboratory, Oak Ridge, Tennessee 37831*
(Received 20 September 2000; published 28 March 2001)

A model has been developed to describe x-ray scattering from CuPt-type ordered III-V ternary semiconductor alloys. The model takes into account the size distribution of the two different laminae-shaped variants, the random distribution of antiphase domain boundaries in each variant, and the atomic displacements due to the bond-length difference between the two constitutive binary materials. A synchrotron x-ray source was employed to measure the weak-ordering reflections from CuPt-ordered $Ga_{0.5}In_{0.5}P$ and $Al_{0.5}In_{0.5}As$ samples. By comparing the experimental results and the model calculations, structure information, including the average number of atomic layers in the laminae of each variant, the average antiphase domain size, and the average order parameter in each variant, were obtained. Results from single-variant films and poorly ordered films are also discussed.

DOI: 10.1103/PhysRevB.63.155310 PACS number(s): 68.55.−a, 61.10.−i, 68.65.−k

## I. INTRODUCTION

III-V semiconductor ternary alloys $A_xB_{1-x}C$ grown on (001)-oriented substrates are known to exhibit CuPt-B-type ordering with one or two ordering variants, i.e., the $[\bar{1}11]$ variant and the $[1\bar{1}1]$ variant, depending on the growth conditions.[1–5] The properties of CuPt-ordered III-V alloys have been extensively studied in the past decade. Many interesting phenomena, such as band-gap reduction,[6] valence-band splitting,[7] optical anisotropy,[8] conductivity anisotropy,[9] second-harmonic generation[10] etc., have been explored by many investigators. It is also known that two-variant ordered films have very different electronic and optical properties from those of one-variant ordered films.[2,11] These studies have revealed that the physical properties of the ordered films depend strongly on the structural details of the material. Extensive transmission electron diffraction (TED) and microscopy (TEM) studies have successfully depicted most of the intrinsic features of the ordered phase, as well as the complex morphologies within the ordered film over a large range of length scales.[12] However, most of these results remain qualitative or, even, inferential. Extended x-ray-absorption fine-structure analyses give quantitative information about the local atomic structure.[13,14] These results indicate that, except for nearest neighbors, which are subject to a microscopic strain, the virtual-crystal approximation can be applied to the alloy crystals. Recently, attempts were published to model the electron-diffraction data on a microscopic scale by employing rather simplified model structures; the results, while informative from a qualitative point of view, are, nontheless, unsatisfactory quantitatively.[15,16]

X-ray diffraction has long been used for a quantitative study of ordering in bulk alloys.[17] However, it has not really been applied to compound semiconductor films except for the recent work of Forrest and co-workers.[18,19] This is mainly because the ordering reflections from the film are weak, and the actual ordered structures are complicated, particularly when two ordering variants coexist. In this paper, we show, by using intense synchrotron x rays and developing a proper structural model that considers both the coexistence of two ordering variants and their complex interplay with randomly distributed antiphase domain boundaries, many interesting diffraction phenenmona can be understood quantitatively. Effects of *A*-*C* and *B*-*C* bond-length differences on the diffraction profiles are also considered in our model, which, as will be demonstrated in the paper, has a strong impact on the determination of the order parameter.

This paper is organized as follows. After the introduction, results of TED and TEM on the CuPt-ordered $A_xB_{1-x}C$ materials will be briefly reviewed in Sec. II. Experimental procedures are given in Sec. III. In Sec. IV, a structural model and a kinematical x-ray-diffraction theory are described. The effects of atomic displacements due to the bond-length difference between *A*-*C* and *B*-*C* bonds on the diffraction data are discussed in Sec. V. Results of the synchrotron x-ray diffraction from our $GaInP_2$ and $AlInAs_2$ films and their interpretations, are presented in Sec. VI. In Sec. VII, we discuss the problems in determining the order parameter from the ordering reflections. Conclusions of this study are given in Sec. VIII.

## II. RESULTS FROM TED AND TEM STUDIES

A typical TED pattern from an ordered $A_xB_{1-x}C$ film with double variants is shown in Fig. 1. The ordering reflections are elongated along directions $\sim 10°$ away from the [001] direction, forming a characteristic *wavy* pattern. The cause of this unusual diffraction phenomenon is believed to be the complex structure of the ordered film, which allows the two variants to interlock with the antiphase domain boundaries to form platelike domains slightly inclined with respect to the [001] direction.[12,20,21] In Fig. 2, atomic images taken from a single-phase, double-variant domain and a single-phase, single-variant domain are shown. In the case of double variants, a laminar structure with alternating variants

 

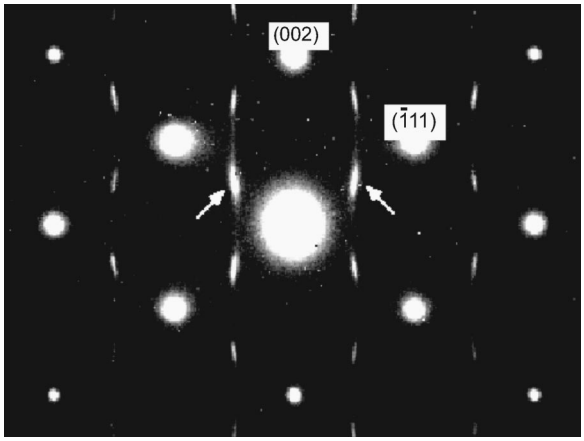


FIG. 1. A typical [110]-zone TED pattern taken from a CuPt-B-type ordered III-V semiconductor alloy. In addition to the fundamental reflection spots, tilted and streaky ordering reflection spots are also seen at $(h/2,k/2,l/2)$ positions.

along the [001] direction is clearly observed. A detailed description of the laminar structure of the two variants and their interlock with the antiphase domain boundaries can be found in Ref. 12, and references therein.

### III. SAMPLE PREPARATION AND X-RAY DIFFRACTION

Samples studied in this work are nominally $Ga_{0.5}In_{0.5}P$ grown on GaAs(001) substrates and $Al_{0.5}In_{0.5}As$ grown on InP(001) substrates by metal-organic chemical vapor deposition. The substrates are tilted by about 6° toward either the $\{111\}A$ or $\{111\}B$ direction. X-ray diffraction was performed on beamline X14A of the National Synchrotron Light Source at the Brookhaven National Laboratory, with an energy of 8.0478 keV. A Si(111) monocromator set slightly away from the Bragg position, and a pulse height analyzer, were used to remove the higher-order harmonics $(\lambda_n=\lambda/n)$. This consideration is particularly important for our experiments because the second-order harmonic would appear exactly at the positions where the ordering reflection would occur [although, in principle, there is no Si(222) reflection, a weak one can be actually measured due to a loss in inversion symmetry of the binding electrons]. A proportional counter was used to record the diffracted x rays. A noncoplanar diffraction geometry (i.e., the plane of diffraction defined by the incident and the diffracted beams is not perpendicular to the sample surface) was introduced in our experiments by using the $\chi$ angle on a standard four-circle diffractometer, so that the reflections, such as $(\bar{1}11)$ and $(\bar{3}/2\ 3/2\ 3/2)$, which are usually not accessible in a conventional coplanar diffraction geometry, can be reached. This noncoplanar geometry is schematically shown in Fig. 3. The incident slits, 0.1 (in plane) $\times 0.5$ mm$^2$ (out of plane), and the receiving slits, 0.5 (in plane) $\times 0.5$ mm$^2$ (out of plane), give a resolution of the diffractometer of about 0.006 in dimensionless reciprocal-lattice units. A post-measurement intensity correction, considering the effective size of the footprint of the incident x-ray beam on the sample surface, is necessary if the scan range is large.

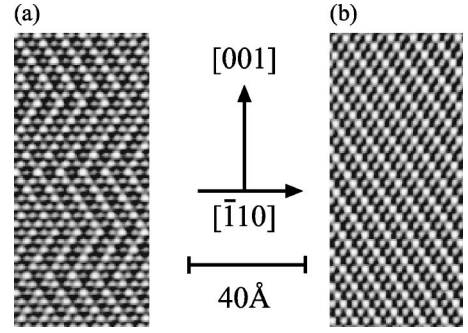


FIG. 2. High-resolution images taken from (a) a double-variant domain and (b) a single-variant ordered domain, by TEM.

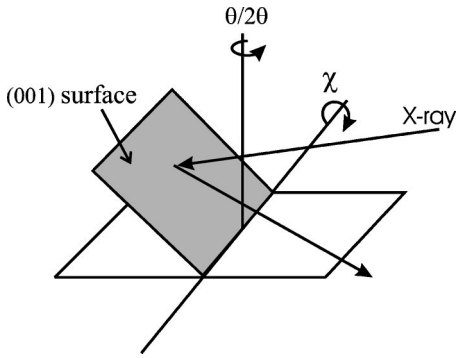


FIG. 3. Schematic diagram showing the diffractometer setup for x-ray measurements.

### IV. STRUCTURAL MODEL AND DIFFRACTION THEORY

The two possible CuPt ordering variants are schematically shown in Figs. 4(a) and 4(b), respectively. In the text of the paper, we will call the $(\bar{1}11)$ and $(1\bar{1}1)$ variants variants I and II, respectively. In the diagram of variant I, an antiphase

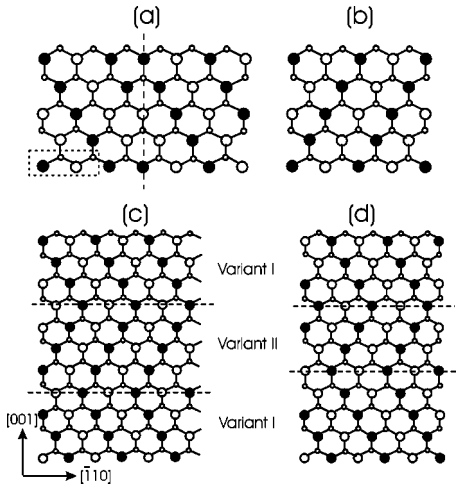


FIG. 4. Schematic diagrams showing the CuPt-ordered structure. (a) Variant I with an antiphase domain boundary. (b) Variant II. (c) and (d) are laminar structures with alternating variants. The lamina of variant II has an even (odd) number of group-III atomic layers in (c) and (d), respectively. Consequently, the adjoining laminae of variant I are in phase and out of phase in (c) and (d), respectively. The dashed rectangle marks the unit cell used in our model.

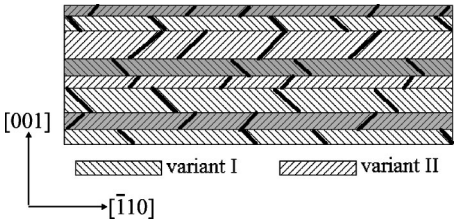


FIG. 5. Structural model of a double-variant film containing randomly distributed antiphase domain boundaries and a random number of atomic layers in each lamina. The thick bars represent the antiphase domain boundaries. Shaded and unshaded laminae of the same variant are out of phase.

domain boundary perpendicular to the $[\bar{1}10]$ direction is also shown. Such boundaries will inevitably exist in the film, because the initial occupation of a group-III lattice site by atom *A* or *B* is equally possible, and the growth actually occurs simultaneously everywhere over the substrate surface. In Figs. 4(c) and 4(d), two examples of a laminar structure with alternating variants are shown. The difference between Figs. 4(c) and 4(d) lies in the thickness of the variant-II lamina, and the effect this has on the relationship between the neighboring variant-I laminae. When the two variant I laminae are separated by a lamina of variant II containing an *even* number of group-III atomic layers [as in Fig. 4(c)], the variant-I laminae are in phase with each other. Conversely, if the intervening variant II lamina is an *odd* number of group-III atomic layers in thickness [(e.g., Fig. 4(d)], the variant-I laminae will then be out of phase. In a real case, the number of group-III atomic layers in a lamina of either variant may be random.

Based on these considerations, a realistic structural model must consist of statistically distributed lateral antiphase domains and a varying phase relationship in the growth direction, as shown in Fig. 5, where the antiphase domains in the two variants are considered to be independent from each other. The number of atomic layers in each lamina is random.

To describe the diffraction theory in steps, let us first neglect the antiphase domain boundaries in the $[\bar{1}10]$ direction, the atomic layers in the $[\bar{1}10]$ direction are assumed to be infinite. The basic structural units that constitute the ordered phase are a layer of group-III atoms and a layer of group-V atoms. In order to obtain a structure of variant I, we have to shift the next group-III atomic layer with respect to the previous one by a vector $(-a/2,0,a/2)$ in the crystallographic coordinate system. The phase shift in the structure factor of this layer caused by such an operation is

$$\alpha = e^{\pi i(q_1+q_3)}, \tag{1}$$

where $(q_1,q_2,q_3)$ are the coordinates of the scattering vector **Q**:

$$\mathbf{Q} = \frac{2\pi}{a}(q_1,q_2,q_3).$$

Similarly, the phase shift between the structure factors of neighboring atomic layers in variant II is

$$\beta = e^{\pi i(-q_1+q_3)}. \tag{2}$$

Let us assume a vertical sequence of *N* pairs of laminae of variants I and II. The *j*th pair of laminae consists of $n_{Aj}$ and $n_{Bj}$ atomic layers of group-III atoms in variants I and II, respectively. These numbers are random. If we denote the structure factors of infinite layers in variants I and II as $F_{0A,B}(\mathbf{Q})$, the structure factor of the whole stack of laminae is then given by

$$F(\mathbf{Q}) = \sum_{j=1}^{N}\left[F_{0A}(\mathbf{Q})\frac{\alpha^{n_{Aj}}-1}{\alpha-1} + F_{0B}(\mathbf{Q})\beta\alpha^{n_{Aj}-1}\frac{\beta^{n_{Bj}}-1}{\beta-1}\right] \times(\alpha\beta)^{j-1}\prod_{k=1}^{j-1}\alpha^{n_{Ak}-1}\beta^{n_{Bk}-1}. \tag{3}$$

The x-ray intensity scattered by such a structure can thus be written in the form

$$\begin{aligned} I(\mathbf{Q}) \propto \langle |F(\mathbf{Q})|^2\rangle = \sum_{j=1}^{N}\Bigg\langle \Bigg| & F_{0A}(\mathbf{Q})\frac{\alpha^{n_{Aj}}-1}{\alpha-1} \\ & + F_{0B}(\mathbf{Q})\beta\alpha^{n_{Aj}-1}\frac{\beta^{n_{Bj}}-1}{\beta-1}\Bigg|^2\Bigg\rangle \\ & + 2\,\mathrm{Re}\Bigg[\sum_{j=2}^{N}\sum_{r=1}^{j-1}(\alpha\beta)^{j-r}\Bigg\langle\Bigg(F_{0A}(\mathbf{Q})\frac{\alpha^{n_{Aj}}-1}{\alpha-1} \\ & + F_{0B}(\mathbf{Q})\beta\alpha^{n_{Aj}-1}\frac{\beta^{n_{Bj}}-1}{\beta-1}\Bigg)\Bigg(F_{0A}(\mathbf{Q})\frac{\alpha^{n_{Ar}}-1}{\alpha-1} \\ & + F_{0B}(\mathbf{Q})\beta\alpha^{n_{Ar}-1}\frac{\beta^{n_{Br}}-1}{\beta-1}\Bigg)^* \\ & \times\prod_{k=r}^{j-1}(\alpha^{n_{Ak}-1}\beta^{n_{Bk}-1})\Bigg\rangle\Bigg]. \end{aligned} \tag{4}$$

Here $\langle\,\rangle$ indicates an average over all possibilities of $n_{Aj}$ and $n_{Bj}$. We denote $\chi_\alpha = \langle\alpha^{n_{Aj}}\rangle$, and $\chi_\beta = \langle\beta^{n_{Bj}}\rangle$ and Eq. (4) can be written as:

$$\begin{aligned} I(\mathbf{Q}) \propto 2N\Bigg\{ & |F_{0A}(\mathbf{Q})|^2\frac{1-\mathrm{Re}(\chi_\alpha)}{|1-\alpha|^2} + |F_{0B}(\mathbf{Q})|^2\frac{1-\mathrm{Re}(\chi_\beta)}{|1-\beta|^2} \\ & - \mathrm{Re}\Bigg(F_{0A}(\mathbf{Q})F_{0B}^*(\mathbf{Q})\frac{1-\chi_\alpha^*}{1-\alpha^*}\frac{1-\chi_\beta^*}{1-\beta}\Bigg)\Bigg\} \\ & + 2\,\mathrm{Re}\Bigg\{\Bigg[|F_{0A}(\mathbf{Q})|^2\alpha\chi_\beta\Bigg(\frac{1-\chi_\alpha}{1-\alpha}\Bigg)^2 \\ & + |F_{0B}(\mathbf{Q})|^2\beta\chi_\alpha\Bigg(\frac{1-\chi_\beta}{1-\beta}\Bigg)^2 + [F_{0A}^*(\mathbf{Q})F_{0B}(\mathbf{Q})\beta\chi_\alpha\chi_\beta \\ & + F_{0A}(\mathbf{Q})F_{0B}^*(\mathbf{Q})\alpha]\frac{1-\chi_\alpha}{1-\alpha}\frac{1-\chi_\beta}{1-\beta}\Bigg]\frac{\chi_\alpha\chi_\beta}{1-\chi_\alpha\chi_\beta} \\ & \times\Bigg(N-1-\frac{1-(\chi_\alpha\chi_\beta)^{N-1}}{1-\chi_\alpha\chi_\beta}\Bigg)\Bigg\}. \end{aligned} \tag{5}$$

If we assume that the numbers $n_{Aj}$ and $n_{Bj}$ follow a Poisson distribution with mean values $\langle n_{Aj}\rangle = n_\alpha$ and $\langle n_{Bj}\rangle = n_\beta$, we obtain

$$\chi_\gamma = e^{-n_\gamma(1-\gamma)}, \quad \gamma = \alpha, \beta. \tag{6}$$

Let us now take into account the lateral antiphase domains in each lamina. In this case, each lamina contains alternating segments out of phase with respect to each other. For the sake of simplicity, we assume that the lateral sequence of these segments is statistically not correlated to the vertical sequence of the two variants. Then the existence of the lateral antiphase domains affects only the terms $|F_{0A}(\mathbf{Q})|^2$, $|F_{0B}(\mathbf{Q})|^2$, and $F_{0A}(\mathbf{Q})F^*_{0B}(\mathbf{Q})$ in Eq. (5). Now these terms must be replaced by their averages, taking into account a sequence of randomly distributed lateral segments. If we further assume that the lateral structures of different laminae are not correlated, then we simply need to make the following replacements in Eq. (5):

$$|F_{0A}(\mathbf{Q})|^2 \rightarrow \langle |F_{0A}(\mathbf{Q})|^2\rangle, \quad |F_{0B}(\mathbf{Q})|^2 \rightarrow \langle |F_{0B}(\mathbf{Q})|^2\rangle,$$

$$F_{0A}(\mathbf{Q})F^*_{0B}(\mathbf{Q}) \rightarrow \langle F_{0A}(\mathbf{Q})\rangle \langle F_{0B}(\mathbf{Q})\rangle^*. \tag{7}$$

The structure factor of the $p$th lateral segment of a layer is shifted by a phase factor $\phi$ with respect to the segment $p-1$,

$$\phi = e^{\pi i(-q_1+q_2)} \equiv e^{-2\pi i q_1},$$

if we assume $q_1 = q_2$ in the $[\bar{1}10]$ scattering plane. The structure factor of such a sequence of segments is

$$F_{0S}(\mathbf{Q}) = \sum_{p=1}^{M} F^{(p)}_{0S}\phi^{p-1}, \quad S = A, B, \tag{8}$$

where

$$F^{(p)}_{0S} = F_{cS}\frac{\phi^{2m_p}-1}{\phi^2-1}\prod_{k=1}^{p-1}\phi^{2m_k}, \quad S = A, B \tag{9}$$

is the structure factor of the $p$th segment of variant-I or -II lamina containing $m_p$ unit cells, M is the number of segments in one lamina, and $F_{cS}$ is the structure factor of one unit cell as defined in Fig. 4. We therefore have

$$\begin{aligned}\langle |F_{0S}(\mathbf{Q})|^2\rangle = |F_{cS}(\mathbf{Q})|^2 \Bigg[ & \sum_{p=1}^{M}\left\langle \left| \frac{\phi^{2m_p}-1}{\phi^2-1}\right|^2\right\rangle \\ & + 2\,\mathrm{Re}\Bigg( \sum_{p=2}^{M}\sum_{k=1}^{p-1}\phi^{p-k}\Bigg\langle \frac{\phi^{2m_p}-1}{\phi^2-1} \\ & \times \left(\frac{\phi^{2m_k}-1}{\phi^2-1}\right)^* \prod_{r=k}^{p-1}\phi^{2m_r}\Bigg\rangle\Bigg)\Bigg], \quad S = A, B.\end{aligned} \tag{10}$$

After some manipulation, we obtain

$$\begin{aligned}\langle |F_{0S}(\mathbf{Q})|^2\rangle = 2\frac{|F_{cS}(\mathbf{Q})|^2}{|\phi^2-1|^2}\Bigg\{ & M[1-\mathrm{Re}(\chi_\parallel)] \\ & - \mathrm{Re}\Bigg[\phi^2\chi_\parallel\frac{(1-\chi_\parallel)^2}{1-\phi\chi_\parallel} \\ & \times\left(M-1-\frac{(\phi\chi_\parallel)^{M-1}-1}{\phi\chi_\parallel-1}\right)\Bigg]\Bigg\},\end{aligned} \tag{11}$$

where

$$\chi_\parallel = \langle \phi^{2m}\rangle \tag{12}$$

is the averaged phase shift over all random numbers $m_p$ of the unit cells in a segment. In a similar way, we obtain

$$\langle F_{0S}(\mathbf{Q})\rangle = F_{cS}(\mathbf{Q})\frac{1-\chi_\parallel}{1-\phi^2}\frac{1-(\phi\chi_\parallel)^M}{1-\phi\chi_\parallel}, \quad S = A, B. \tag{13}$$

The averaged phase shift $\chi_\parallel$ can be calculated readily if we assume that the random numbers of $m_p$ follow a Poisson distribution with an average $\langle m_p\rangle \equiv m$:

$$\chi_\parallel = e^{-m(1-\phi^2)}. \tag{14}$$

Different configurations of antiphase domain boundaries can now be achieved by different combinations of the parameters $n_\alpha$, $n_\beta$, and $m$.

## V. EFFECT OF THE ATOMIC DISPLACEMENTS

Bulk semiconductor alloys $A_xB_{1-x}C$ are known to obey Vegard's law quite accurately: the *overall* lattice constant is the average of the bulk $AC$ and $BC$ lattice constants, weighted by mole fraction. If we imagine the alloy to be a *virtual crystal* (VC), in that each atom sits on geometrically precise zinc-blende lattice sites, then its lattice constant can be expressed as

$$a_{ABC} = x a_{AC} + (1-x)a_{BC}.$$

Indeed, measurements[13,14] show that the second-nearest-neighbor distances between group-III atoms (or between group-V atoms) in the lattice are very nearly those $-a_{ABC}/\sqrt{2}-$ expected for such a VC approximation.

In contrast, however, first-nearest-neighbor distances between group-III and -V atoms deviate significantly from $\sqrt{3}a_{ABC}/4$, expected from the VC approximation. It is always that the $A$-$C$ (or $B$-$C$) bond length is shorter (or longer) than the VC bonds. Therefore, one can imagine that, instead of occupying the VC lattice sites, the atoms will sit in positions slightly deviated from the VC sites, resulting in a *microscopic strain* in the alloy. Such deviations or microscopic strain have been treated in great detail in the past 20 years, employing mainly what are known as valence-force-field models,[22–24] in which the energies of individual bonds and bond angles are considered to be independent of each other. By minimizing the total energy of the typical tetrahedral bond structure in diamond-type semiconductors, the actual bond lengths, or the first-nearest-neighbor distances, and the displacements of the atoms from their VC sites, can be de-

termined. For most of the common semiconductor alloys, values of the actual bond lengths in differently ordered structures can be widely found in the literature.[22,23,25]

Now let us discuss the effect of such atomic displacements on the x-ray-diffraction intensity. For an ordered crystal, the structure factor $F_{cS}$ of a unit cell can be written in a general form

$$F_{cS}=\sum_i f_i(\mathbf{r_i})e^{2\pi i\mathbf{Q}\cdot(\mathbf{r_i}+\delta_\mathbf{i})}, \tag{15}$$

where

$$f_i(\mathbf{r_i})=\overline{f_i}+f(\mathbf{r_i})$$

is composed of two components, the mean atomic form factor $\overline{f_i}$ of a disordered crystal at lattice site $\mathbf{r_i}$ in the VC approximation, and the deviation of the atomic form factor from $\overline{f_i}$ at $\mathbf{r_i}$ due to the atomic ordering, $f(\mathbf{r_i})$. $\delta_\mathbf{i}$ is the displacement of the atom at $\mathbf{r_i}$. The summation in Eq. (15) is over all the atomic sites $\mathbf{r_i}$ in the unit cell. The exponential term in Eq. (15) can be expanded to

$$e^{2\pi i\mathbf{Q}\cdot\mathbf{r_i}}(1+2\pi i\mathbf{Q}\cdot\delta_\mathbf{i}),$$

assuming that $\delta_\mathbf{i}$ is much smaller than the VC bond length. To obtain the x-ray intensity, we have to calculate the average of $|F_{cS}|^2$ over all possiblities of atom arrangements due to ordering, and all the possibilites of the atomic displacements. If we assume that the atomic form factors for the atoms at different lattice sites and the displacements of the atoms at these sites are not correlated, and further assume that $f_i(\mathbf{r_i})$ and $\delta_\mathbf{i}$ at the same site are independent variables (note that the displacement of an atom at $\mathbf{r_i}$ depends mainly on its first-nearest neighbors, and is rather an intrinsic property of the $ABC_2$-type semiconductor alloys than a result of atomic ordering), then we have

$$\begin{aligned}\langle|F_{cS}|^2\rangle&=\left\langle\sum_i\sum_j f_i(\mathbf{r_i})f_j^*(\mathbf{r_j})e^{2\pi i\mathbf{Q}\cdot(\mathbf{r_i}+\delta_\mathbf{i})}e^{-2\pi i\mathbf{Q}\cdot(\mathbf{r_j}+\delta_\mathbf{j})}\right\rangle\\&\simeq\left\langle\sum_i\sum_j f_i(\mathbf{r_i})f_j^*(\mathbf{r_j})e^{2\pi i\mathbf{Q}\cdot(\mathbf{r_i}-\mathbf{r_j})}(1+2\pi i\mathbf{Q}\cdot\delta_\mathbf{i})\right.\\&\quad\left.\times(1-2\pi i\mathbf{Q}\cdot\delta_\mathbf{j})\right\rangle\\&=\sum_i\sum_j\langle f_i(\mathbf{r_i})\rangle\langle f_j(\mathbf{r_j})\rangle^*e^{2\pi i\mathbf{Q}\cdot(\mathbf{r_i}-\mathbf{r_j})}\\&\quad\times(1+2\pi i\mathbf{Q}\cdot\langle\delta_\mathbf{i}\rangle)(1-2\pi i\mathbf{Q}\cdot\langle\delta_\mathbf{j}\rangle)\\&\simeq\sum_i\sum_j\langle f_i(\mathbf{r_i})\rangle\\&\quad\times\langle f_j(\mathbf{r_j})\rangle^*e^{2\pi i\mathbf{Q}(\mathbf{r_i}+\langle\delta_\mathbf{i}\rangle)}e^{-2\pi i\mathbf{Q}(\mathbf{r_j}+\langle\delta_\mathbf{j}\rangle)}.\end{aligned} \tag{16}$$

Therefore, the effect of the ordering and atomic displacements on the x-ray scattering can be taken into account by replacing the atomic form factors and the atom displacements in Eq. (15) by their averages.

Now Eq. (15) can be rewritten as

$$F_{cS}=\sum_i\langle f_i(\mathbf{r_i})\rangle e^{2\pi i\mathbf{Q}\cdot(\mathbf{r_i}+\langle\delta_\mathbf{i}\rangle)}. \tag{17}$$

It can also be written in the form

$$\begin{aligned}F_{cS}&=\sum_i\{\overline{f_i}+\langle f(\mathbf{r_i})\rangle+2\pi i\mathbf{Q}\cdot\langle\delta_i\rangle[\overline{f_i}+\langle f(\mathbf{r_i})\rangle]\}e^{2\pi i\mathbf{Q}\cdot\mathbf{r_i}}\\&=F_0+F_s+F_d,\end{aligned} \tag{18}$$

where

$$F_0=\sum_i\overline{f_i}e^{2\pi i\mathbf{Q}\cdot\mathbf{r_i}}, \tag{19}$$

$$F_s=\sum_i\langle f(\mathbf{r}_i)\rangle e^{2\pi i\mathbf{Q}\cdot\mathbf{r_i}}, \tag{20}$$

$$F_d=2\pi i\sum_i\mathbf{Q}\cdot\langle\delta_\mathbf{i}\rangle[\overline{f_i}+\langle f(\mathbf{r_i})\rangle]e^{2\pi i\mathbf{Q}\cdot\mathbf{r_i}} \tag{21}$$

are the contributions to the total structure factor from a perfect VC, from atomic ordering and from atomic displacements, respectively. The x-ray intensity is calculated by

$$\begin{aligned}|F_{cS}|^2&=(F_0+F_s+F_d)(F_0^*+F_s^*+F_d^*)\\&=F_0F_0^*+F_sF_s^*+2\,\mathrm{Re}(F_0F_s^*)+2\,\mathrm{Re}(F_dF_0^*)\\&\quad+2\,\mathrm{Re}(F_dF_s^*)+F_dF_d^*.\end{aligned} \tag{22}$$

The first term in Eq. (22) gives the fundamental reflections. The second term is caused by the atomic ordering. The third term is zero because $\Sigma_i f(\mathbf{r_i})=0$. The fourth and fifth terms result in diffuse intensities around the fundamental and ordering reflections, respectively. The last term, though much weaker than the other terms, represents the contribution purely due to the atomic displacements. In our case, because the displacements are also ordered, as we will show in the following discussion, the atomic displacements bring in an additional modulation to the ordering reflections. Therefore, the intensity of an ordering reflection from a single variant domain is

$$I_{order}\propto|F_s|^2+2\,\mathrm{Re}(F_dF_s^*)+|F_d|^2. \tag{23}$$

In addition to the bond-length-difference-induced permanent atom displacements, the thermal vibration of the atoms causes a random displacement. The effect of this thermal vibration on the x-ray structure factor is considered via Debye-Waller factors. In this paper, the Debye-Waller factors were calculated from the estimated Debye temperatures,[26,27] using the Debye model, resulting in $B_{InP}=0.2799$, $B_{GaP}=0.3001$, $B_{InAs}=0.206$, and $B_{AlAs}=0.283$.

Before calculating the average atomic form factor and the average atom displacements, let us introduce the well-accepted Bragg-Williams long-range order parameter $s$.[17] If we define $\gamma_A(\gamma_B)$ and $\omega_A(\omega_B)$ as the fraction of $A$ sites ($B$ sites) occupied by the right and wrong atoms, respectively, we then have

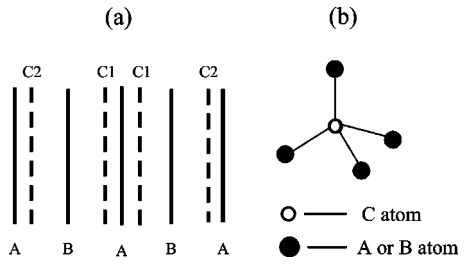


FIG. 6. (a) Schematic diagrams of the ordered $(\bar{1}\bar{1}1)$ lattice planes considering the atomic displacements due to the bond-length difference between *A*-*C* and *B*-*C* in an $A_{0.5}B_{0.5}C$ alloy. The *C* lattice planes have been sorted into two types, $C1$ and $C2$, based on their displacements due to the bond-length difference between *A*-*C* and *B*-*C*. (b) The tetrahedron bonding in a diamond-type structure. Distributions of *A* and *B* atoms on the four bonding positions depend on the ordering of the alloy.

$$s=\gamma_A+\gamma_B-1=\gamma_A-\omega_B=\gamma_B-\omega_A. \tag{24}$$

For simplicity, here we will discuss only the case in which the mole fractions of *A* and *B* atoms in the alloy are equal. Our results, however, can easily be extended to the general case where *A* and *B* atoms have different mole fractions. Bearing this in mind, the possibilities of finding the right and wrong atoms at group-III lattice sites are $P_\eta=\gamma_\eta/(\gamma_\eta+\omega_\eta)$ and $1-P_\eta$, respectively, where $\eta=A,B$. Therefore, the average atomic form factors for *A* and *B* sites are

$$\bar{f}(A)=\frac{1}{2}(f_A+f_B)+\frac{s}{2}(f_A-f_B),$$

$$\bar{f}(B)=\frac{1}{2}(f_A+f_B)+\frac{s}{2}(f_B-f_A). \tag{25}$$

The calculation of the average atomic displacements is more complicated. In an $A_xB_{1-x}C$ alloy, VFF model calculation indicates that mainly the group-V atoms have been displaced to accommodate the bond-length difference. In a disordered phase, the group-III atoms *A* and *B* are randomly distributed, so that the average atom displacement for each lattice site is zero. If *A* and *B* atoms form CuPt-type ordering, however, they will prefer to reside on alternating $(\bar{1}\bar{1}1)$ or $(1\bar{1}\bar{1})$ lattice planes. Consequently, the displacements of the atoms *C* form a periodic pattern, they move closer to either the *A*-rich lattice plane or the *B*-rich lattice plane depending on which of the *A*-*C* and *B*-*C* bonds is shorter, as shown schematically in Fig. 6(a). In this way, we can sort the atoms *C* into two types, type 1 and type 2, as indicated in Figs. 6(a). For each tetrahedral structure with an atom *C* sitting in the center, there are 16 possibilities to displace this atom depending on the occupation of the four atoms *A* and *B* bonding directly to it [Fig. 6(b)]. Considering all these 16 different atom arrangements and their possibilities, we finally obtain the magnitude of the average displacements of type-1 and -2 lattice *C* planes as

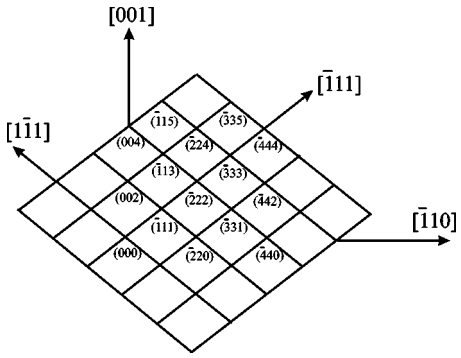


FIG. 7. The reciprocal-space area within which most of the experimental measurements were made in this work.

$$|\delta|=\left[\left(\frac{1+s_\tau}{2}\right)^4-\left(\frac{1-s_\tau}{2}\right)^4\right]d_t+\left(\frac{1+s_\tau}{2}\right)\left(\frac{1-s_\tau}{2}\right)\left[\left(\frac{1+s_\tau}{2}\right)^2-\left(\frac{1-s_\tau}{2}\right)^2\right]d_s, \tag{26}$$

where $\tau=1$ and 2, corresponding to the variants I and II, respectively, $d_t$ and $d_s$ are parameters determined from a separate VFF model calculation. For different materials, they have different values. The direction of the average displacements are perpendicular to the ordered $\{111\}$ latice planes. In Sec. VI, we will show how this displacement influences the diffraction profiles.

## VI. RESULTS AND DISCUSSION

In this section, we present and discuss the experimental results and theoretical fitting results for several $Ga_{0.5}In_{0.5}P$ and $Al_{0.5}In_{0.5}As$ films, which are quite representative of the CuPt-type ordered III-V semiconductor alloys. Samples MA776 and MA912 are $Ga_{0.5}In_{0.5}P$ films grown on GaAs (001)-6°*A* substrates. Sample K782 is a $Ga_{0.5}In_{0.5}P$ film grown on an InP(001)-6°*B* substrate. Sample R286 is an $Al_{0.5}In_{0.5}As$ film grown on an exactly oriented InP(001) substrate. Growth conditions of the $Ga_{0.5}In_{0.5}P$ films and the $Al_{0.5}In_{0.5}As$ film can be found in Refs. 11 and 18, respectively. Figure 7 is a schematic diagram of the [110]-zone reciprocal-lattice plane within which most of the scans in this work were made. It is well known that a film grown on a substrates miscut toward the (111)-*B* direction would result in single variant in the film.[1–6] In such a case, only one set of the ordering reflections were observed by TED. No wavy or tilted ordering peaks were observed in such films. Our x-ray measurements on sample K782 indeed confirm that only one variant appears in this film grown on a 6°*B* substrate. The measured reciprocal area map of this sample around $(\bar{3}/2,3/2,5/2)$ ordering reflection is shown in Fig. 8(a). The intensities of the fundamental reflections and their tails in the measured area have been subtracted from the map in order to highlight the rather weak ordering peak. This procedure has been performed on all the data discussed below. The peak in Fig. 8(a) does indeed look close to a circle as already noticed by TED observations. Figure 8(b) is the calculated $(\bar{3}/2,3/2,5/2)$ reflection. Figure 8(c) shows the cross section

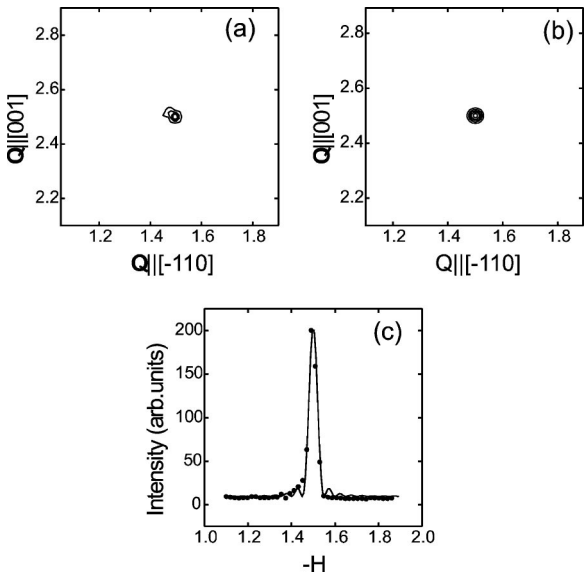


FIG. 8. X-ray reciprocal-space area maps taken from a single-variant film: (a) experimental, (b) calculated, and (c) cross-sectional line scans at $\mathbf{Q}_{\|}[001]=2.5$.

at $\mathbf{Q}_{\|}[001]=2.5$. The best agreement between the calculated and measured data was achieved by using a domain size of about 500 crystallographic unit cells. Here it is worth pointing out that the intensities of the ordering reflections have been modulated by the effect of atomic displacements as discussed in Sec. V. As an example, Fig. 9 shows the calculated x-ray radial scans from reciprocal lattice points $(\bar{1}11)$ to $(\bar{3}33)$ for a perfectly ordered large single-variant domain. The central peak in each panel is the fundamental $(\bar{2}22)$ reflection. Figure 9(a) is the result without taking into account the atomic displacements. Naturally, the $(\bar{3}/2,3/2,3/2)$ reflection is stronger than the higher-order $(\bar{5}/2,5/2,5/2)$ reflection, as the atomic form factor decreases with increasing scattering vector. In Fig. 9(b), scattering due to the atomic displacements is shown, which gives a modulation to the above profile. In Fig. 9(c), the total intensity profile considering the atom displacements is shown. The $(\bar{5}/2,5/2,5/2)$ reflection here is considerably stronger than the $(\bar{3}/2,3/2,3/2)$ reflection.

Figure 10(a) is an experimental x-ray area scan in reciprocal space taken from sample MA776 around the ordering reflections $(\bar{7}/2,7/2,5/2)$ and $(\bar{7}/2,7/2,7/2)$. It is clear that both ordering peaks are inclined away from the [001] direction by an angle of about 10°. This feature is quite similar to the typical TED data shown in Fig. 1. It is easy to recognize that the $(\bar{7}/2,7/2,7/2)$ and $(\bar{7}/2,7/2,5/2)$ reflections are contributions of the ordering variants I and II, respectively. We also note that the reflection $(\bar{7}/2,7/2,7/2)$ is much stronger than the reflection $(\bar{7}/2,7/2,5/2)$. However, we must not conclude from this feature that the fraction of the variant I in this sample is larger than that of the variant II. Figure 10(b) gives the calculated intensity distribution by using Eq. (5). The parameters used for the calculation are listed in Table I. Both maps agree qualitatively quite well but for a detailed com-

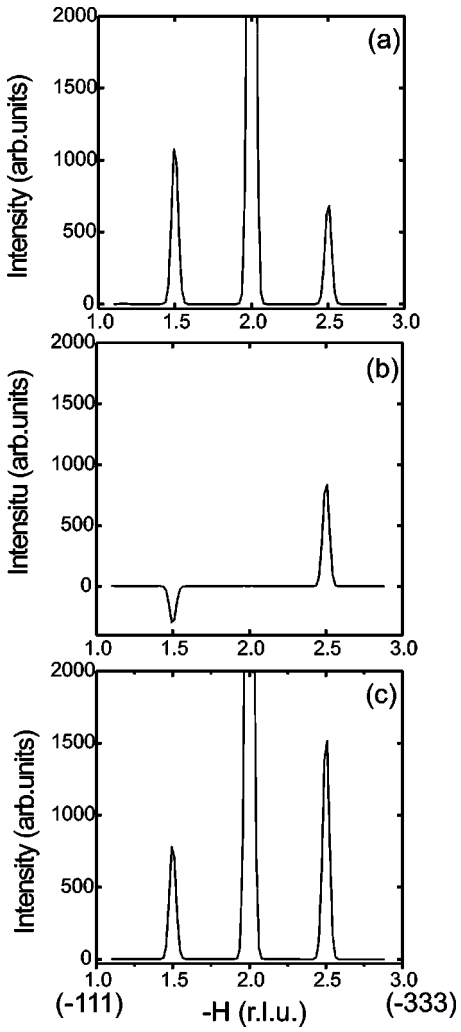


FIG. 9. Calculated x-ray line scans from reciprocal-space lattice points $(\bar{1}11)$ to $(\bar{3}33)$. (a) Without taking into account the atomic displacements. (b) Modulation caused by atomic displacements. (c) Results of (a)+(b).

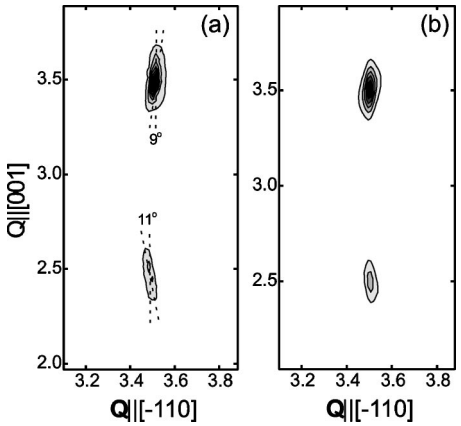


FIG. 10. X-ray reciprocal space area scans of sample MA776: (a) experiment; (b) calculation. The peaks centered at $(\bar{7}/2,7/2,7/2)$ and $(\bar{7}/2,7/2,5/2)$ are attributed to variants I and II, respectively.

TABLE I. The parameters used to fit the measured data of samples MA776, MA912, and R286. $\langle n_\alpha \rangle$, $\langle n_\beta \rangle$, and $\langle m \rangle$ are the average number of group-III atomic layers in the laminae of variants I and II, and the average antiphase domain size. $\langle s_1 \rangle$ and $\langle s_2 \rangle$ are the average order parameters of variants I and II, respectively.

| Sample | $\langle n_\alpha \rangle$ | $\langle n_\beta \rangle$ | $\langle m \rangle$ | $\langle s_1 \rangle$ | $\langle s_2 \rangle$ |
|---|---|---|---|---|---|
| MA776 | 7 | 8 | 60 | $0.35 \pm 0.05$ | $0.45 \pm 0.05$ |
| MA912 | 12 | 12 | 140 | $0.50 + 0.05$ | $0.50 + 0.05$ |
| R286 | 4 | 4 | $\sim$ | $0.30^a \pm 0.05$ | $0.30^a \pm 0.05$ |

[a]For ordered domains only.

parison of the calculation and the experiment, area maps are not suitable. In Figs. 11(a) and 11(b), two cross sections at $\mathbf{Q}_\parallel[001] = 2.5$ and 3.5 are shown. We see that the theory yields a quite good fit to the experimental data. In Fig. 12, a fit, using the same parameters, to a line scan from reciprocal lattice point $(\bar{1}13)$ to $(\bar{3}\bar{3}5)$ is shown, and the agreement is also good increasing our confidence in the model.

Figure 13(a) shows the experimental area map taking from sample MA912. Figure 13(b) is the calculated one using Eq. (5). The structural parameters used for this calculation are listed in Table I. To view quantitatively the fitting results, several line scans along either $[\bar{1}11]$ or $[1\bar{1}1]$ directions are shown in Fig. 14, namely, scans from the reciprocal lattice point $(\bar{1}11)$ to $(\bar{3}\bar{3}3)$, (002) to $(\bar{2}\bar{2}0)$, $(\bar{1}\bar{1}3)$ to $(\bar{3}\bar{3}1)$, and (002) to $(\bar{2}\bar{2}4)$. Good agreement has been obtained between the several experimental and simulated curves.

From the calculations, we note that the widths of the ordering reflections are determined by the combination of lateral antiphase domain size and the laminar thicknesses, i.e., the overall configuration of the antiphase domain boundaries. This is also true for the tilt angle of the ordering reflections. To show this point more clearly, a series of calculated area scans using a $Ga_{0.5}In_{0.5}P$ film as the model structure are shown in Figs. 15 and 16. By varying the average thicknesses of the laminae of the two variants and the lateral domain size, we are able to obtain quite different diffraction patterns. From Fig. 15, we notice that when the antiphase domains are very small in size, each ordering reflection has split into two. The smaller the antiphase domains, the greater the separation of the two split maxima are located. In fact, such splittings of ordering reflections and shifts of intensity maxima have been observed by TED on poorly ordered

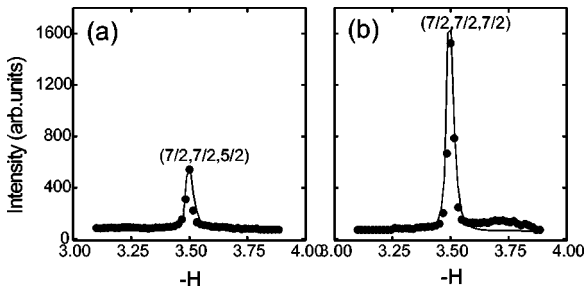


FIG. 11. Cross-sectional line scans through the peak maxima in Fig. 10 at (a) $Q_\parallel[001] = 2.5$ and (b) $Q_\parallel[001] = 3.5$.

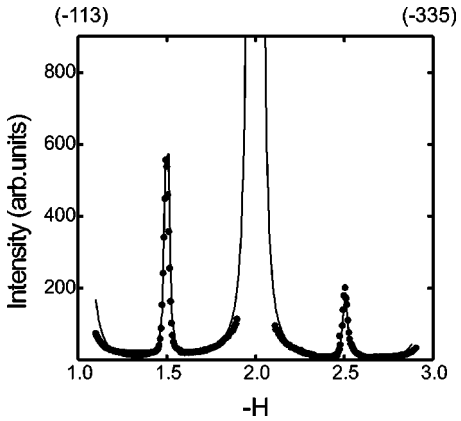


FIG. 12. X-ray line scans from reciprocal-lattice points $(\bar{1}13)$–$(\bar{3}\bar{3}5)$. The solid dots and the line are measured and calculated results, respectively.

films[12] (the TED pattern in Fig. 1 is an example of such a case). It is also clear that when the antiphase domains are very large, the ordering reflections become very narrow and lie almost parallel to the [001] direction. This latter finding is further confirmed by Fig. 16(d), which represents an area scan for a two-variant structure without lateral antiphase domains but with statistically distributed laminae thicknesses. In this case, the ordering reflection is elogated simply along the [001] direction, but is no longer tilted to form the wavy pattern. Therefore, dense antiphase domain boundaries are responsible for the tilted reflection peaks.

Not all of the films, however, are well ordered, by which we mean that the two ordered variants are complementary in the film. Some films grown under certain conditions may not be well ordered, in which ordered domains are embedded in the disordered matrix.[15,28] In this case, TEM study has shown that the ordered domains have a finite lateral size, but, in the [001] direction, the ordering develops quite well. Overall, these ordered domains are characterized by a columnar structure.[15] Based on the theory first developed by Greenholz

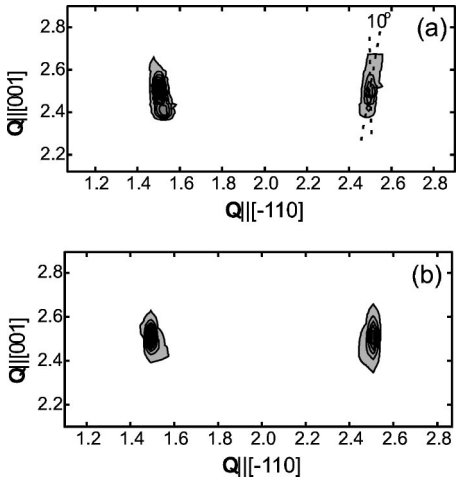


FIG. 13. X-ray reciprocal-space area scans of sample MA912: (a) experiment; (b) calculation. The peaks centered at $(\bar{5}/2,5/2,5/2)$ and $(\bar{3}/2,3/2,5/2)$ are attributed to variants I and II, respectively.

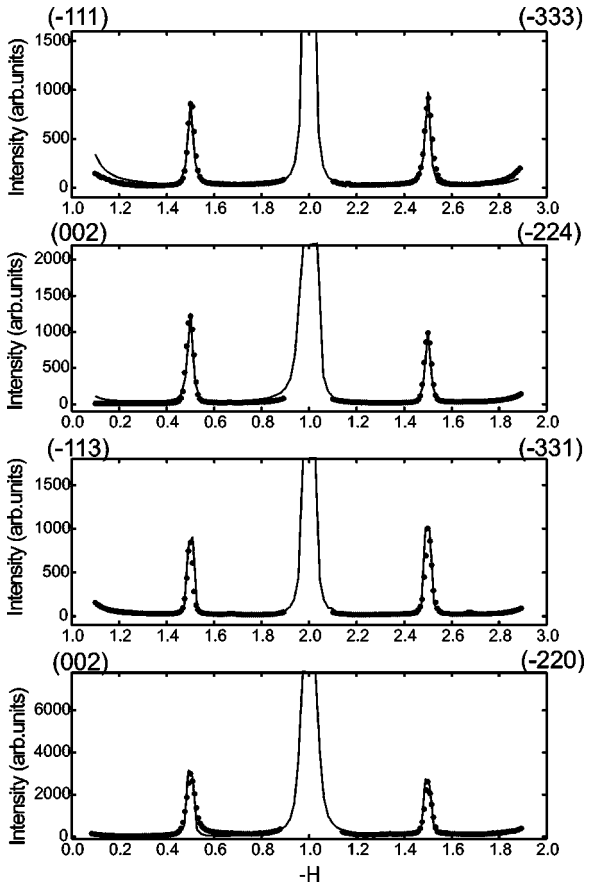


FIG. 14. X-ray line scans from one reciprocal-lattice point to another. (a) From $(\bar{1}\bar{1}1)$ to $(\bar{3}\bar{3}3)$. (b) From (002) to $(\bar{2}\bar{2}4)$. (c) From $(\bar{1}\bar{1}3)$ to $(\bar{3}\bar{3}1)$. (d) From (002) to $(\bar{2}\bar{2}0)$. Solid dots and lines are measured and calculated data, respectively.

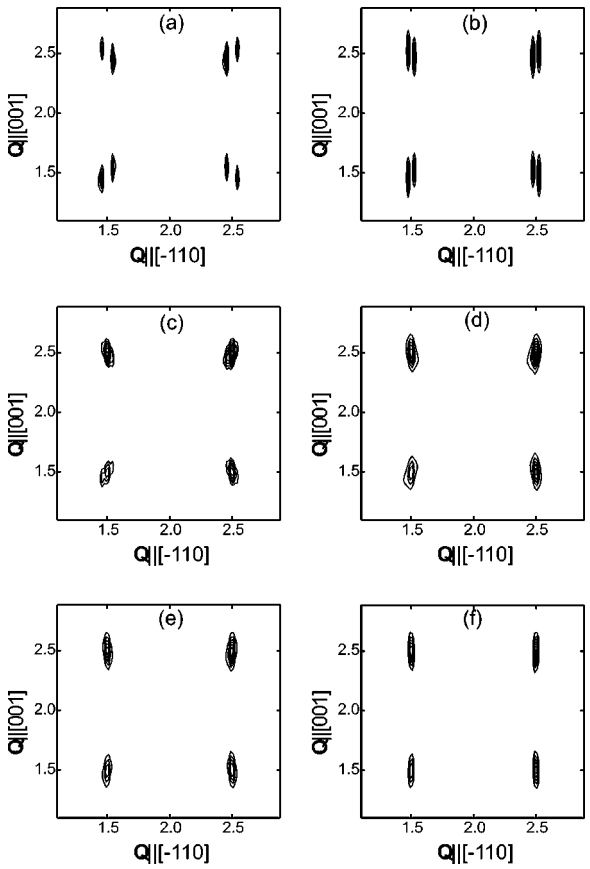


FIG. 15. A series of calculated area scans for an ordered $Ga_{0.5}In_{0.5}P$ model structure with the parameters $\langle n_\alpha \rangle = \langle n_\beta \rangle = 8$ and (a) $\langle m \rangle = 5$, (b) $\langle m \rangle = 10$, (c) $\langle m \rangle = 20$; (d) $\langle m \rangle = 40$, (e) $\langle m \rangle = 60$, and (f) $\langle m \rangle = 200$.

and Kidron,[29] in which the interference between the scattering from different ordered domains is neglected, we can calculate the x-ray scattering intensity from a columnar structure by keeping the same vertical structural model, as we used above for the well ordered materials. Figure 17(a) is a reciprocal-space area scan taken from sample R286. This sample was shown to exhibit short-range order from our earlier work.[18] The general feature of this figure, particularly the inclination of the streaks passing through the $(\bar{h}/2,k/2,l/2)$ positions, is quite similar to that of the well-ordered materials. The elongated streaks are clear indications of small ordering domains in the film. An interesting feature here is the presence of streaks parallel to the [001] direction, running between the ordering reflections. [The ridge of intensity between $(\bar{3}\bar{3}1)$ and $(\bar{1}\bar{1}3)$ is due to the high density of planer stacking faults. See Ref. 18 for details.] Figure 17(b) is the calculated area map using the columnar structure model and the parameters listed in Table I. It fits qualitatively quite well to Fig. 17(a), considering the shape and tilt of the ordering reflections, as well as the [001] streaks between them. In fact, the quantative fit is also good if we show cross-sectional line scans running through the ordering peaks (Fig. 18). We see from Fig. 18 that both the line shape and intensity of the calculated curves are in good agreement with their experi-

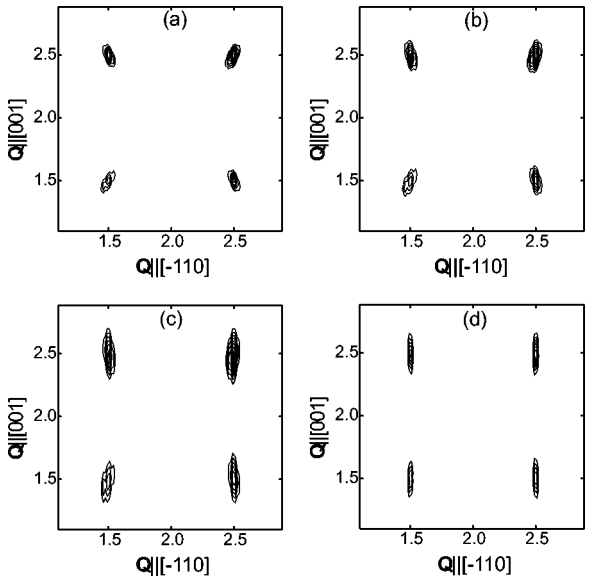


FIG. 16. Calculated area scans for an ordered $Ga_{0.5}In_{0.5}P$ model structure with the structural parameters $\langle m \rangle = 20$ and (a) $\langle n_\alpha \rangle = \langle n_\beta \rangle = 12$, (b) $\langle n_\alpha \rangle = \langle n_\beta \rangle = 8$, and (c) $\langle n_\alpha \rangle = \langle n_\beta \rangle = 4$. (d) is calculated by using $\langle n_\alpha \rangle = \langle n_\beta \rangle = 8$, and assuming that the film is free of lateral anti-phase-domain boundaries.

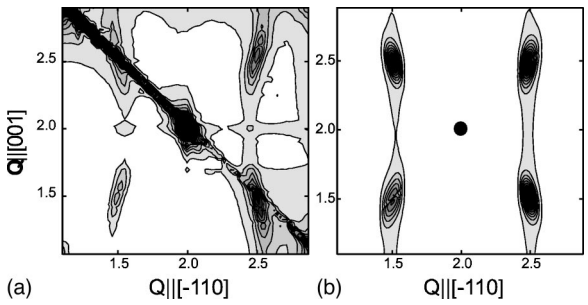


FIG. 17. X-ray reciprocal-space area scans of sample R286. (a) Experimental. (b) Calculated by using a columnar structural model.

mental counterparts. Note that no antiphase domain boundaries were considered in the columnar model. This implies that antiphase domain boundaries are not necessary to cause the wavy diffraction pattern for the poorly ordered films. The same conclusion was also reached by Yang *et al.* in a recent work.[15] The stronger $(\bar{5}/2,5/2,5/2)$ reflection in comparison with the $(\bar{3}/2,3/2,3/2)$ reflection is again due to the atomic displacements.

## VII. ON THE DETERMINATION OF THE ORDER PARAMETER

Conventionally, the order parameter is determined by comparing the intensities of the ordering and fundamental reflections weighted by their structure factors.[17–19] Even without considering the structural details of the ordered material, this method has already encountered several difficulties when applied to the CuPt-type ordered thin films. For example, a precise determination of the intensity of a fundmental reflection is often difficult. This is because the film is usually lattice matched to the substrate material, and the reflections from the substrate and film overlap one another. However, many researchers, including us, have used this method in earlier studies.[30,31] There is no doubt that this method will produce correct values for good single crystals of a pure variant if the intensity of the fundamental reflections can be determined correctly.

However, as we have discussed in previous sections, the intensity of the ordering reflection is not only a function of the order parameter, but is also modulated by the atomic displacements. The almost inevitable presence of antiphase

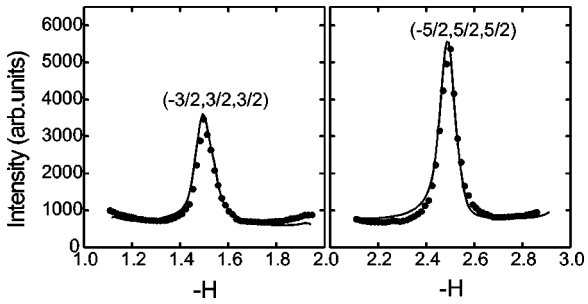


FIG. 18. Cross-sectional line scans through the reciprocal-lattice points $(\bar{3}/2,3/2,3/2)$ and $(\bar{5}/2,5/2,5/2)$ in Fig. 17. Solid dots and lines are measured and calculated data, respectively.

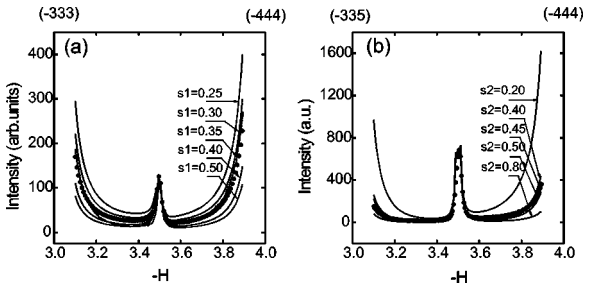


FIG. 19. Theoretical simulations of two line scans of sample MA776 from reciprocal-lattice points $(\bar{3}33)$ to $(\bar{4}44)$ and $(\bar{3}35)$ to $(\bar{4}44)$ across the ordering reflections of variants I and II, respectively. The best fits were obtained by using an order parameter of $0.35\pm0.05$ for variant I and an order parameter of $0.45\pm0.05$ for variant II.

domains in the ordered phase leads to an additional phase factor in the structure factor calculation, which may again have significant impact on the intensity of the ordering reflections. In order to determine the order parameter correctly, all these factors need to be considered. The best way to do this, therefore, is to fit the experimental x-ray profiles using a model which takes into account all these factors. Figure 19 shows, as an example, detailed theoretical fittings to the measured x-ray intensity profiles for sample MA776. The calculated curves here are normalized with respect to the intensity of the corresponding ordering peak. It is seen that the best fit was obtained with the average order parameters of $0.35\pm0.05$ for variant I and $0.45\pm0.05$ for variant II. We also note that the calculated and measured curves deviate considerably at the tails of the fundamental reflections. We believe this is caused by the fact that the actual structure of the film is more complicated than our model, which permits us to include static displacement diffuse scattering near the fundamental peaks (Huang scattering). In addition, the actual film may contain defects such as diffuse antiphase domain boundaries,[12] stacking faults,[18] alloy clustering[15,32] etc. The interface of the neighboring laminae of the two variants may also not be as abrupt as we considered in our model. It is worth pointing out that the order parameter of sample MA776, determined from a direct comparison of the intensities of the $(\bar{1}/2,1/2,3/2)$ ordering reflection and the (004) fundamental reflection using the methods discussed in Ref. 30, is about 0.06 for both variants, taking the volume fractions of the two variants determined in Sec. VI.

Finally, we note that the precise determination of the order parameter for the complex ordered film by diffraction methods is still a challenge. Our model assumes that the laminar structure runs uniformly across the wafer, and the number of atomic layers in a single lamina follows a certain distribution. Such assumptions may not be always true. Electron diffraction may indeed be better in determing the local order parameter if one can focus the electron beam onto a single-phase, single-variant domain, and use kinematic theory (always a problem with TED).

## VIII. CONCLUSIONS

On the basis of a theory of kinematic diffraction and a structure model of CuPt-type ordering in III-V compound

semiconductors, considering the laminae structure of two alternating variants and the random distribution of antiphase domain boundaries in each variant, we have calculated the reciprocal-space distribution of the x-ray intensities scattered from CuPt-type ordered $A_xB_{1-x}C$ materials. Atomic displacements due to the bond-length difference between *A*-*C* and *B*-*C* were also considered in our model. We find that, since atomic displacements are associated with atomic ordering, the average atomic displacements of alternating 111 lattice planes are also ordered. This gives an additional modulation to the intensity of the ordering reflections. Several samples of $Ga_{0.5}In_{0.5}P$ and $Al_{0.5}In_{0.5}As$ have been studied experimentally employing synchrotron x-ray radiation. By comparing the experimental and calculated x-ray reciprocal area maps, the structural parameters of the films, such as the mean domain size, the mean thickness of the laminae of both variants, and the average order parameter have been determined.

## ACKNOWLEDGMENTS

This work was supported by the NSF, Grant No. DMR-9729297 and the Texas Center for Superconductivity at the University of Houston (TcSUH). NREL is a national laboratory operated by Midwest Research Institute, Battelle, and Bechtel, for the U.S. Dept. of Energy under Contract No. DE-AC36-99GO10337. V. H. acknowledges the travel support granted by the University of Houston. We thank D. J. Friedman and J. M. Olsen (NREL) for preparing the samples.

[1] D. H. Jaw, G. S. Chen, and G. B. Stringfellow, Appl. Phys. Lett. **59**, 114 (1991).
[2] Y. Zhang, B. Fluegel, S. P. Ahrenkiel, D. J. Friedman, J. F. Geisz, J. M. Olsen, and A. Mascarenhas (unpublished).
[3] L. C. Su, I. H. Ho, and G. B. Stringfellow, J. Appl. Phys. **75**, 5135 (1994).
[4] I. J. Murgatroyd, A. G. Norman, and G. R. Booker, J. Appl. Phys. **67**, 2310 (1990).
[5] T. Suziki and A. Gomyo, J. Cryst. Growth **93**, 396 (1988).
[6] A. Gomyo and T. Suzuki, Phys. Rev. Lett. **60**, 2645 (1988).
[7] A. Mascarenhas, S. Kurtz, A. Kibbler, and J. M. Olsen, Phys. Rev. Lett. **63**, 2108 (1989).
[8] F. A. J. M. Driessen, G. J. Bauhuis, P. R. Hageman, A. van Geelen, and L. J. Giling, Phys. Rev. B **50**, 17 105 (1994).
[9] J. Novak, S. Hasenohrl, R. Kudela, M. Kucera, D. Wullner, and H.-H. Wehmann, Appl. Phys. Lett. **73**, 369 (1998).
[10] B. Fluegel, A. Mascarenhas, J. F. Geisz, and J. M. Olsen, Phys. Rev. B **57**, R6787 (1998).
[11] Y. Zhang, A. Mascarenhas, S. P. Ahrenkiel, D. J. Friedman, J. F. Geisz, and J. M. Olsen, Solid State Commun. **109**, 99 (1999).
[12] C. S. Baxter, W. M. Stobbs, and J. H. Wilkie, J. Cryst. Growth **112**, 373 (1991), and references therein.
[13] D. C. Meyer, K. Richter, and P. Paufler, Phys. Rev. B **59**, 15 253 (1999).
[14] L. Alagna, T. Properi, S. Turchini, C. Ferrari, L. Francesio, and P. Franzosi, J. Appl. Phys. **83**, 3552 (1998).
[15] J.-J. Yang, R. Spirydon, T.-Y. Seong, S. H. Lee, and G. B. Stringfellow, J. Electron. Mater. **27**, 1117 (1998).
[16] D. Munzer, E. Dobrocka, I. Vavra, R. Kudela, M. Harvanka, and N. E. Christensen, Phys. Rev. B **57**, 4642 (1998).
[17] B. E. Warren, *X-Ray Diffraction* (Dover, New York, 1990).
[18] J. Kulik, R. L. Forrest, T. D. Golding, and S. C. Moss, J. Mater. Res. **15**, 45 (2000).
[19] R. L. Forrest, in *Spontaneous Ordering in Semiconductor Alloys*, edited by A. Mascarenhas (Plenum, New York, 2000).
[20] E. Morita, M. Ikeda, and O. Kumagai, Appl. Phys. Lett. **53**, 2164 (1988).
[21] G. S. Chen, D. H. Jaw, and G. B. Stringfellow, J. Appl. Phys. **69**, 4263 (1991).
[22] Y. Cai and M. F. Thorpe, Phys. Rev. B **46**, 15 872 (1992); **46**, 15 879 (1992).
[23] J. S. Chung and M. F. Thorpe, Phys. Rev. B **55**, 1545 (1997).
[24] J. Y. Tsao, *Materials Fundamentals of Molecular Beam Epitaxy* (Academic Press, San Diego, 1993), Chap. 4.
[25] A.-B. Chen and A. Sher, *Semiconductor Alloys* (Plenum Press, New York, 1995).
[26] S. Adachi, *Physical Properties of III-V Semiconductor Compounds* (Wiley, New York, 1992).
[27] S. Adachi, *Properties of Aluminum Gallium Arsenide* (INSPEC, London, 1993).
[28] T.-Y. Seong, A. G. Norman, G. R. Booker, and A. G. Cullis, J. Appl. Phys. **75**, 7852 (1994).
[29] M. Greenholz and A. Kidron, Acta Crystallogr., Sect. A: Cryst. Phys., Diffr., Theor. Gen. Crystallogr. **26**, 311 (1970).
[30] R. L. Forrest, T. D. Golding, S. C. Moss, Z. Zhang, J. F. Geisz, J. M. Olsen, A. Mascarenhas, P. Ernst, and C. Geng, Phys. Rev. B **58**, 15 355 (1998).
[31] C. S. Baxter and W. M. Stobbs, Philos. Mag. A **69**, 615 (1994).
[32] S. Matsumura, K. Takano, N. Kuwano, and K. Oki, J. Cryst. Growth **115**, 194 (1991).